# Self-supervised Signal Denoising for Magnetic Particle Imaging

Huiling Peng[1,2,3], Yimeng Li[1,4], Xin Yang[1,2,3], Jie Tian[1,2] and Hui Hui[1,2,3*]

***Abstract*— Magnetic particle imaging (MPI) is a medical imaging technology with high resolution and high sensitivity, which tracks the distribution of superparamagnetic iron oxide nanoparticles (SPIONs) in the nonlinear response to dynamic excitation at a field-free region. However, various noises distort the signals resulting in a decline in imaging quality. Traditional threshold-based methods cannot remove dynamic noise in MPI signals. Therefore, a self-supervised denoising method is proposed to denoise MPI signals in this study. The approach adopted U-net as the backbone and modified the network for MPI signals. The network is trained using two periods of noisy signals and the shape prior knowledge of the MPI signals is introduced for promoting the convergence of the self-supervised net. The experiments show that the learning-based method can still denoising the MPI signal without labeling data and eventually improve image quality, and our approach can achieve the best performance compared with other self-supervised methods in MPI signal denoising.**

## I. INTRODUCTION

Magnetic particle imaging (MPI) is a tracer-based imaging method. By receiving the nonlinear magnetization response signal of magnetic nanoparticles (MNPs) in the dynamic magnetic field, the spatial distribution of MNPs is determined [1], [2]. The principle promises MPI the potential of achieving high spatiotemporal resolution and no radioactive. The method has already shown its performance for various medical applications such as cancer detection [3], cell tracking [4], and plaque detection [5].

In the process of MPI signal generation, there is a field-free region (FFR) in a static gradient magnetic field. Then FFR moves in the field-of-view (FOV) by applying a time-varying excitation field. The nonlinear magnetization response of MNPs in the FFR generates a high-frequency harmonic signal. The voltage signal is received by the receive coil. In this process, various factors raise the detection limit [6]. There is noise in the receive chains following a Gaussian statistic. Besides, non-linear electronic components in the scanner system generate harmonic interference which is often superimposed into the particle signal. Conventionally, MPI signal noise is reduced by background subtraction [7]. The particle signal is obtained by measuring the noise with an empty scanner and subtracting the noise from particle measurements. This method cannot handle dynamic changes in the background signal from a measurement.

[1]CAS Key Laboratory of Molecular Imaging, Institute of Automation, Beijing, China

[2]Beijing Key Laboratory of Molecular Imaging, Beijing, China

[3]School of Artificial Intelligence, University of Chinese Academy of Sciences, Beijing, China

[4]School of Engineering Medicine and School of Biological Science and Medical Engineering, Beihang University, Beijing, China

* Corresponding author hui.hui@ia.ac.cn

Recently, with the development of deep learning, learning-based methods have shown superior performance than traditional methods and it is also gradually applied in the field of MPI [8], [9], [10]. Relevant methods for improving MPI resolution require massive noisy-clean data pairs. However, there is no large-scale open MPI signal dataset and it is difficult to obtain a large amount of high-quality MPI signal data. The size of the dataset is usually extended through data enhancement methods such as data rotation, clipping, and partial data exchange. Due to the similar features between MPI signals, the data enhancement is not significantly improved.

In this study, we introduce a self-supervised MPI signal denoising model to extract features from the noisy signal directly and alleviate dependence on clean data while reducing MPI signal noise. Experiments show that our self-supervised method outperforms other self-supervised methods for MPI signal denoising.

## II. METHODS

### A. MPI signal datasets

For MPI system simulation, the MNPs distribution is obtained by upsampling the image in the MNIST dataset. When static gradient magnetic field $G$ and two-way excitation field $f_x$ and $f_y$ are applied [11], the MNPs response signal $\tilde{s}(t)$ was generated as [12]:

$$\tilde{s}(t) = B_1(x) m \rho(x) ** \frac{||\dot{x}_s(t)||}{H_{sat}} h(x) \dot{x}_s(t)|_{x=x_s(t)} \quad (1)$$

where $B_1$ is the sensitivity of receive coil, $m = \frac{\pi d^3 M_{sat}}{6}$ is the magnetic moment of a spherical, single domain magnetic nanoparticle, $d$ and $M_{sat}$ are the diameter and the saturated magnetic moment of MNPs, respectively. $\rho(\cdot)$ is the MNPs density, $x_s(t)$ and $\dot{x}_s(t)$ are the position and the velocity of field free point at time $t$, $h(\cdot)$ is the point spread function. the magnetic saturation field $H_{sat} = \frac{k_b T}{\mu_0 m}$ is given by Boltzmann constant $k_b$, vacuum permeability $\mu_0$, and temperature $T$. '$**$' is the two-dimensional convolutional operation.

Two kinds of noises were added to distort the signals $\tilde{s}(t)$, including Gaussian noise and harmonic interference. The intensity of added Gaussian noise is following the signal-to-noise (SNR):

$$SNR = 20 \log_{10} \frac{\tilde{s}(t)}{\sigma} \quad (2)$$

where $\sigma$ is the standard deviation of added Gaussian noise. In the simulation, harmonic interference is added following the signal-interference-ratio (SIR) [6]:

$$SIR = 20 \log_{10} \frac{S_n(f)}{\gamma} \quad (3)$$

where $S_n(f)$ is the $n^{th}$ harmonic band. $\gamma$ means the uniform distribution that similar to the $\sigma$ in SNR.

### B. Self-supervised learning denoiser

Training a self-supervised neural network regressor using a set of input-target pairs $(s_i, s_j)$ is to find $\hat{s}$ which has the smallest average deviation from the measurements.

$$\arg\min_{\theta} E_{s_i,s_j} L_{reg}(f_\theta(s_i), s_j) \tag{4}$$

Based on the principle, the overview of the designed self-supervised denoising framework for MPI signal denoising is shown in Fig. 1. Two periodical noisy signals $s$ were collected, one cycle $s_1$ is for training, and the other $s_2$ is used as the corresponding target. $s_1$ and $s_2$ have the same MPI response signal amplitude and the noises with the same distribution but different values. When $s_1$ is processed by the self-supervised denoising network $f_\theta(\cdot)$, a predicted signal $f_\theta(s_1)$ is generated. Mean absolute error is used which calculates the pointwise distance between the output and the label defined as followed.

$$L_{reg} = L_1(f_\theta(s_1), s_2) = ||s_1 - s_2||_1 \tag{5}$$

If $f_\theta(s_1)$ is clean, the $L_{reg}$ converges to the minimum. But the denoising task is solved as an inverse problem and the ill-position results in a non-unique solution. Therefore, the prior knowledge of the MPI response signal is introduced to narrow the range of the solution. The MPI response signal of each cycle presents symmetrical distribution.

$$\lim_{\triangle t \to 0} \frac{s_{t+\triangle t} - s_t}{\triangle\, t} = \lim_{\triangle t \to 0} \frac{s_{T-t+\triangle t} - s_{T-t}}{\triangle\, t} \tag{6}$$

Accordingly, gradient difference (GD) loss is designed which calculates the gradient of the first half cycle and the second half cycle of the signal, respectively, and uses their difference as part of the loss.

$$L_{GD} = \sum_{t \in (0, T/2]} s_t^{'} - s_{T-t}^{'} \tag{7}$$

Besides, since the noise is randomly distributed, the $L_{GD}$ is prone to oscillate, and the total variation (TV) loss [13] is used to smooth the edge set.

$$L_{TV} = \sum_{t \in [0, T)} |s_{t+1} - s_t| \tag{8}$$

Therefore, the total loss function is designed as followed:

$$L = L_{reg} + \alpha L_{GD} + \beta L_{TV} \tag{9}$$

where the hype parameters $\alpha$, $\beta$ are used to control the strength of the regularization term in the training scheme.

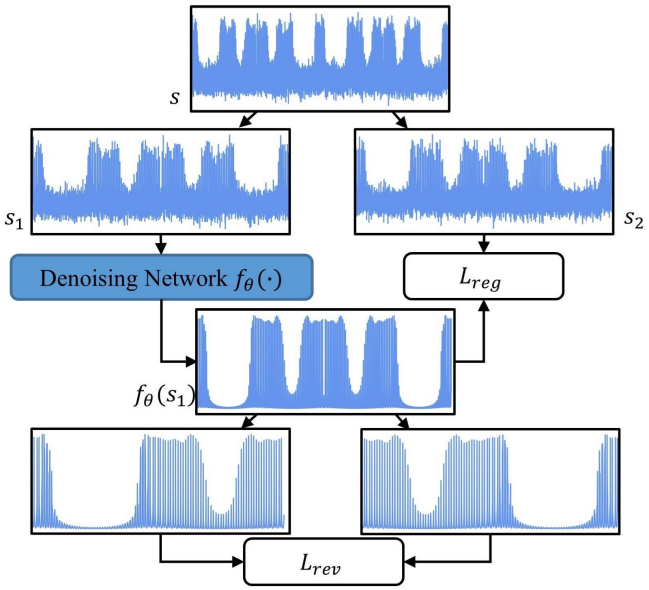


Fig. 1. Overview of our proposed self-supervised framework. Acquiring MPI signal $s$ which includes two periods, one for training named $u_1$ and another used as a label called $s_2$. Then the denoising network $f_\theta(\cdot)$ takes $s_1$ as input and produce the denoised result $f_\theta(s_1)$. The revised loss $L_{rev}$ maintains the symmetrical characteristic of the MPI signal.

### C. Denoising network architecture

U-Net was adopted as the backbone and the structure has been modified as shown in Fig. 2. In the Encoder part, given an input $s(t)$ with the size $1 \times N_0$, the first three layers map the signal to an $C \times N$ feature map, which is then processed by the following four encoder's blocks (EcBs). Each of the EcBs sequentially connects a down-sampling layer, a dropout layer, a parametric rectified linear unit (PReLU), and 3 ResBlocks [14]. Each ResBlock can be described by the following equation

$$F(X) = W_j * (PReLU(W_i * X)) + X \tag{10}$$

where X is the input feature, '$*$' means the convolutional operation and the function of PReLU is

$$f(x) = max(0, x) + \lambda min(0, x) \tag{11}$$

Besides, dropout layers are added before the PReLU layers. In the dropout layer, each weight value is set to zero with a probability $p$. Down-sampling operation is realized using $1 \times 1$ convolutional (Conv) layer with a stride of 3.

The decoder contains four decoder's blocks (DcBs) and an upsampling layer. Each of the DcBs sequentially connects an upsampling layer with a scaling factor of 3, two Conv, and a PReLU. The Concatenation operation in a DcB stacks the feature map from the ResBlock in the corresponding EcB and the one output of the up-sampling layer.

## III. Experiments & Results

### A. Implementation details

For MPI system simulation, cartesian scanning is adopted, and the specific setting parameters of the simulation are shown in Table I.

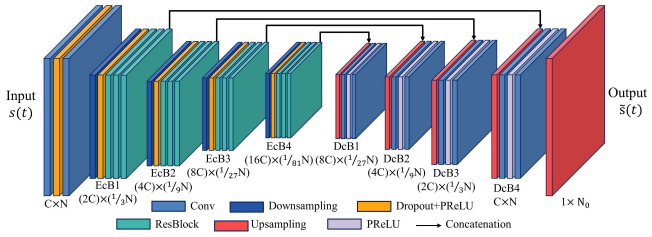


Fig. 2. Architecture of designed denoising network model.

TABLE I

PARAMETERS FOR THE MPI PARTICLE SIGNAL SIMULATION

| Symbol | Parameters | Value | Unit |
|---|---|---|---|
| $d$ | Nanoparticle diameter | 20 | $nm$ |
| $M_{sat}$ | Saturation magnetization | $4.77 \times 10^{-5}$ | $Am^{-1}$ |
| $\mu_0$ | Vacuum permeability | $4\pi \times 10^{-7}$ | $NA^{-2}$ |
| $k_b$ | Boltzmann's constant | $1.38 \times 10^{-23}$ | $JK^{-1}$ |
| $T$ | Temperature | 300 | $K$ |
| $G$ | Selective field gradient | 0.4 | $T/m$ |
| $f_x$ | Excitation frequency in x direction | $2.5 \times 10^3$ | $Hz$ |
| $f_y$ | Excitation frequency in y direction | 500 | $Hz$ |

In experiments, 10000 images from the MNIST test were used as the source of the particle distribution. The images are up-sampled to $101 \times 101$ pixels. After the MPI system simulation, we got 10000 pieces of MPI response signal data with dimension $R^{1\times 9900}$. We randomly divided them into training, verification, and test sets, which contain 8000, 1000, and 1000 signals, respectively. We consider the following five types of synthetic noise distributions: (1) SNR = 15dB, (2) SNR = 10dB, (3) SNR = 5dB, (4) SNR = 15dB, SIR = 15dB, (5) SNR = 15dB, SIR = 5dB.

In training, epochs are set to 100 and AdamW is used as our optimizer. The batch size is set to 2 and the learning rate is 0.0001. The number of features $C$ is set to 48. The dropout rate $p$ is 0.2. $\beta$ is set to 0.01, and $\alpha$ is set to 0.03, 0.08, and 0.5 for types (1-3), (4), and (5), respectively.

### B. Comparisons with state-of-art methods

To evaluate the denoising performance of the proposed framework, it compared with two self-supervised denoisers: Noise2Noise (N2N) [15] and Recorrupted-to-Recorrupted (R2R) [16]. We evaluate the methods from the results of the denoised signal and reconstructed image. SNR and RMSE were used as evaluation criteria in denoised signals. SSIM and PSNR are used in reconstructed images.

The quantitative results are shown in Table II and the comparison example of the denoised signal and the reconstructed image using the x-space algorithm [12] is shown in Fig. 3. It shows that our method performs more adapted to MPI signal denoising tasks than other self-supervised methods. Moreover, with the noise distribution becoming more complex and the signal-related harmonic interference increasing gradually, the performance of R2R drops rapidly, and noise can be better suppressed by GD regularization.

### C. Comparisons on OpenMPIdata

In this section, we constructed the dataset based on the instrument parameters in OpenMPIdata [17], using the

TABLE II

QUANTITATIVE COMPARISON OF DIFFERENT METHODS FOR GAUSSIAN NOISE AND HARMONIC INTERFERENCE.

| Noise type | Methods | SNR | RMSE ($\times 10^{-3}$) | SSIM | PSNR |
|---|---|---|---|---|---|
| Gaussian SNR = 15 dB | Noisy | 15.00 | 40.56 | 0.74 | 30.03 |
| | N2N[15] | 22.78 | 16.87 | 0.95 | 34.48 |
| | R2R[16] | 21.82 | 19.00 | 0.96 | 35.18 |
| | Ours | **26.10** | **11.39** | **0.98** | **37.68** |
| Gaussian SNR = 10 dB | Noisy | 10.00 | 72.13 | 0.56 | 25.41 |
| | N2N[15] | 19.97 | 23.00 | 0.92 | 31.60 |
| | R2R[16] | 16.82 | 33.52 | 0.91 | 29.81 |
| | Ours | **23.83** | **14.79** | **0.97** | **34.72** |
| Gaussian SNR = 5 dB | Noisy | 5.00 | 128.27 | 0.39 | 21.13 |
| | N2N[15] | 16.53 | 34.17 | 0.87 | 28.30 |
| | R2R[16] | 11.68 | 60.50 | 0.69 | 24.90 |
| | Ours | **20.97** | **20.95** | **0.95** | **31.66** |
| Gaussian SNR = 15 dB Interference SIR = 15 dB | Noisy | 12.66 | 53.72 | 0.68 | 27.96 |
| | N2N[15] | 20.94 | 20.91 | 0.94 | 32.67 |
| | R2R[16] | 18.18 | 29.16 | 0.88 | 30.65 |
| | Ours | **25.13** | **12.61** | **0.96** | **34.07** |
| Gaussian SNR = 15 dB Interference SIR = 5 dB | Noisy | 6.20 | 116.33 | 0.47 | 22.58 |
| | N2N[15] | 17.48 | 30.92 | 0.89 | 29.06 |
| | R2R[16] | 8.83 | 88.04 | 0.55 | 23.23 |
| | Ours | **22.72** | **16.59** | **0.94** | **31.46** |

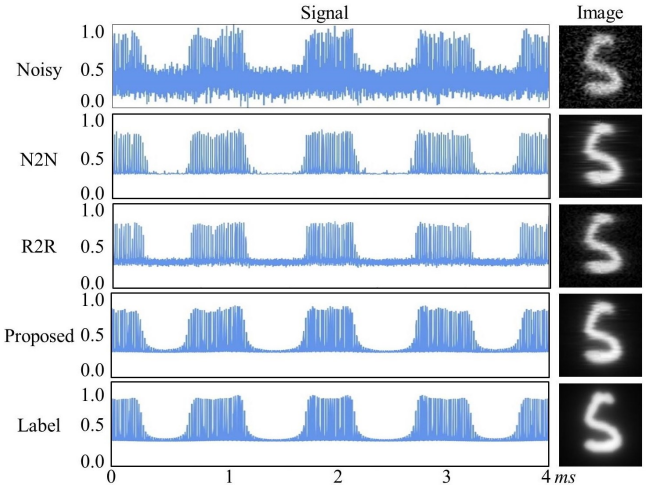


Fig. 3. The comparison of denoised signal and the corresponding reconstructed image using the x-space algorithm.

MNIST test set to make the dataset with a training set size of 8000, a validation set size of 1000, and a testing set size of 1000. The noises added are Gaussian noise with SNR = 15 dB and harmonic interference with SIR = 5 dB. The quantification results are shown in Table III, and the comparison results of the simulated data and OpenMPIdata signals are shown in Fig. 4. The left two columns show the predicted signal results and corresponding reconstructed images of each method on simulated signal data, while the third column shows the denoising results of each method on the concentration phantom signal in OpenMPI data.

### D. Ablation study

Here, we conduct ablation studies to analyze the influence of the regularization terms. All the ablation experiments are completed on the dataset of Gaussian noise with SNR = 5

TABLE III

QUANTITATIVE COMPARISON OF DIFFERENT METHODS FOLLOWING THE PARAMETERS IN OPENMPIDATA.

| Noise type | Methods | SNR | RMSE ($\times 10^{-4}$) | SSIM | PSNR |
|---|---|---|---|---|---|
| Gaussian | Noisy | 4.86 | 54.41 | 0.74 | 19.89 |
| SNR = 15 dB | N2N[15] | 18.88 | 9.58 | 0.93 | 25.32 |
| Interference | R2R[16] | 15.04 | 15.34 | 0.81 | 21.60 |
| SIR = 5 dB | Ours | **24.09** | **5.28** | **0.95** | **26.20** |

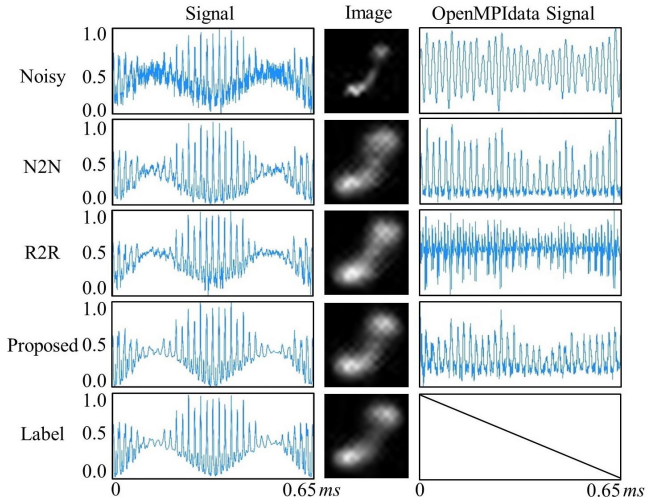


Fig. 4. Comparison of prediction results using different methods. The three columns represent the signals predicted by each method, the reconstructed images corresponding to the signals using the x-space algorithm, and the prediction results of OpenMPIdata signals.

dB. Table IV shows that the GD term increases the SNR but decreases the RMSE. because the GD function focuses on the local areas with large gradients and it reduces the focus on the whole set. When the TV term is introduced, the local influence is weakened, and the network performance is improved more comprehensively.

TABLE IV

THE ABLATION RESULTS OF DIFFERENT REGULARIZATION TERMS

| | SNR | RMSE($\times 10^{-3}$) | SSIM | PSNR |
|---|---|---|---|---|
| $L_1$ | 18.97 | 25.72 | 0.95 | 31.53 |
| $L_1 + \alpha L_{GD}$ | 19.49 | 24.19 | 0.94 | 30.20 |
| $L_1 + \beta L_{TV}$ | 18.89 | 25.92 | 0.94 | 29.35 |
| $L_1 + \alpha L_{GD} + \beta L_{TV}$ | **20.79** | **20.95** | **0.95** | **31.66** |

## IV. CONCLUSIONS

In this study, we proposed a self-supervised MPI signal denoising method trained on noisy signals only. The approach utilizes the features of the noisy signal, realizing the removal of multiple noises. The shape prior knowledge of signal is introduced to improve the denoising performance. The experimental results show that the approach can improve signal quality and the reconstructed image. In the future, the model will be further optimized to improve the extraction of global information features.

## ACKNOWLEDGMENT

This work was supported in part by the National Natural Science Foundation of China under Grant: 62027901.

## REFERENCES

[1] B. Gleich and J. Weizenecker, "Tomographic imaging using the nonlinear response of magnetic particles," *Nature*, vol. 435, no. 7046, pp. 1214–1217, 2005.

[2] T. Knopp, S. Biederer, T. F. Sattel, J. Rahmer, J. Weizenecker, B. Gleich, J. Borgert, and T. M. Buzug, "2d model-based reconstruction for magnetic particle imaging," *Medicle physics*, vol. 37, no. 2, pp. 485–491, 2010.

[3] G. Wang, W. Li, G. Shi, Y. Tian, L. Kong, N. Ding, J. Lei, Z. Jin, J. Tian, and Y. Du, "Sensitive and specific detection of breast cancer lymph node metastasis through dual-modality magnetic particle imaging and fluorescence molecular imaging: a preclinical evaluation," *European Journal of Nuclear Medicine and Molecular Imaging*, vol. 49, no. 8, pp. 2723–2734, 2022.

[4] L. Kiru, A. Zlitni, A. M. Tousley, G. N. Dalton, W. Wu, F. Lafortune, A. Liu, K. M. Cunanan, H. Nejadnik, T. Sulchek, M. E. Moseley, R. G. Majzner, and H. E. Daldrup-Link, "In vivo imaging of nanoparticle-labeled car t cells," *Proceedings of the National Academy of Sciences*, vol. 119, no. 6, p. e2102363119, 2022.

[5] W. Tong, H. Hui, W. Shang, Y. Zhang, F. Tian, Q. Ma, X. Yang, J. Tian, and Y. Chen, "Highly sensitive magnetic particle imaging of vulnerable atherosclerotic plaque with active myeloperoxidase-targeted nanoparticles," *Theranostics*, vol. 11, no. 2, pp. 506–521, 2021.

[6] P. Hendrik, K. Olaf, W. James, L. Norbert, and W. Frank, "Characterization of noise and background signals in a magnetic particle imaging system," *Physics in Medicine and Biology*, vol. 65, no. 23, p. 235031, 2020.

[7] K. Them, M. G. Kaul, C. Jung, M. Hofmann, T. Mummert, F. Werner, and T. Knopp, "Sensitivity enhancement in magnetic particle imaging by background subtraction," *IEEE Transactions on Medical Imaging*, vol. 35, no. 3, pp. 893–900, 2016.

[8] A. Güngör, B. Askin, D. A. Soydan, E. U. Saritas, C. B. Top, and T. Çukur, "Transms: Transformers for super-resolution calibration in magnetic particle imaging," *IEEE Transactions on Medical Imaging*, vol. 41, no. 12, pp. 3562–3574, 2022.

[9] Y. Shang, J. Liu, L. Zhang, X. Wu, P. Zhang, L. Yin, H. Hui, and J. Tian, "Deep learning for improving the spatial resolution of magnetic particle imaging," *Physics in Medicine and Biology*, vol. 67, no. 12, p. 125012, 2022.

[10] X. Wu, B. He, P. Gao, P. Zhang, Y. Shang, Z. Liwen, J. Zhong, J. Jiang, H. Hui, and J. Tian, "Pgnet: Projection generative network for sparse-view reconstruction of projection-based magnetic particle imaging," *Medical physics*, 2022.

[11] L. Yin, W. Li, Y. Du, K. Wang, Z. Liu, H. Hui, and J. Tian, "Recent developments of the reconstruction in magnetic particle imaging," *Visual Computing for Industry, Biomedicine, and Art*, vol. 5, no. 1, p. 24, 2022.

[12] P. W. Goodwill and S. M. Conolly, "Multidimensional x-space magnetic particle imaging," *IEEE Transactions on Medical Imaging*, vol. 30, no. 9, pp. 1581–1590, 2011.

[13] M. Storath, C. Brandt, M. Hofmann, T. Knopp, J. Salamon, A. Weber, and A. Weinmann, "Edge preserving and noise reducing reconstruction for magnetic particle imaging," *IEEE Transactions on Medical Imaging*, vol. 36, no. 1, pp. 74–85, 2017.

[14] Z. Wu, C. Shen, and A. van den Hengel, "Wider or deeper: Revisiting the resnet model for visual recognition," *Pattern Recognition*, vol. 90, pp. 119–133, 2019.

[15] J. Lehtinen, J. Munkberg, J. Hasselgren, S. Laine, T. Karras, M. Aittala, and T. Aila, "Noise2Noise: Learning image restoration without clean data," in *Proceedings of the 35th International Conference on Machine Learning (ICML)*, 2018, pp. 2965–2974.

[16] T. Pang, H. Zheng, Y. Quan, and H. Ji, "Recorrupted-to-recorrupted: Unsupervised deep learning for image denoising," in *2021 IEEE/CVF Conference on Computer Vision and Pattern Recognition (CVPR)*, 2021, pp. 2043–2052.

[17] T. Knopp, P. Szwargulski, F. Griese, and M. Gräser, "Openmpidata: An initiative for freely accessible magnetic particle imaging data," *Data in Brief*, vol. 28, p. 104971, 2020.